Smart Agricultural Technology 12 (2025) 101399

Contents lists available at ScienceDirect

Smart Agricultural Technology

journal homepage: www.journals.elsevier.com/smart-agricultural-technology

A deep learning model to time-profile plant nutrient uptake in a growth accelerator

Matthew R. Redding *, Armando J. Navas Borrero

Department of Primary Industries, 203 Tor Street Toowoomba, Queensland, Australia

ARTICLE INFO

Keywords:
3D plant scanning
Nutrient synchronisation
Plant method
Deep learning
Enhanced efficiency fertiliser

ABSTRACT

Synchrony between nutrient supply and plant demand is a key performance indicator of enhanced efficiency fertilisers (EEF's). This study sought to develop a high throughput technique for rapid, non-destructive plant biomass measurements. In three experiments, a 3D camera mounted on a robotic gantry scanned pots weekly. A deep learning neural network (RandLA-net) was trained with colour point cloud (PCD) data to isolate a single central plant from partly overlapping adjacent plants and infrastructure (overall testing accuracy of 0.93 and mean intersection over union, IOU, of 0.90). Segmented voxel counts were strongly related to above ground dry matter ($R^2 = 0.87$; $P < 2.2e\text{-}16$), and key statistics related to nutrient synchrony, for example inflection point of the logistic growth curve, were successfully measured. The high-throughput technique allowed rapid evaluation of fertiliser treatment performance and relative nutrient synchrony over time. Optimisation of the approach can be achieved by careful model plant selection, limiting target nutrient applications to less than that required for growth to plateau, and including a maximal productivity reference.

Introduction

The value of synchronising nutrient availability with plant requirements is evident. Precise application of fertiliser nutrients at time points synchronised with crop demand can substantially decrease system losses and increase nutrient use efficiency [1,2]. While incremental in-season fertiliser additions are unlikely to be applicable to all mechanised production systems [3], formulation of EEF's may provide similar benefits [3–5].

Therefore, a key performance indicator of EEF's is their ability to sparingly meet the target plant's nutrient demand throughout the growing season. This implies that an efficient and realistic means of measuring nutrient delivery throughout the growing season is required. One method, release of nutrients from EEF's into water, though widely assessed by materials experts [6,7], is poorly related to agronomic performance and nutrient losses [8]. Another approach previously employed has been the use of sequential pasture cuts, a labour intensive process, limited to providing uptake data points on a two to three week frequency with attendant analysis delays [3].

Significant success has been achieved using above ground biomass measurement via three dimensional imagery (3D) to identify relative differences between the performance of different EEF formulations compared to conventional fertilisers [8]. Scanning in 3D was chosen for this work, rather than calculation from two dimensional images, to provide an effective means of calculating the size of plant when the upper canopy tends to obscure lower stems and leaves from a single camera position. In their study, Redding et al. [8] resorted to a classical artificial intelligence technique (Kth-nearest neighbour clustering) based on voxel colour (specified as hue, saturation, and value) and elevation. This provided estimates of dry matter production with an R^2 of 79 % ($P < 2.2 \times 10^{-16}$). Assessment of each of these scans was an investment of at least several hours of work.

To enable scanning and calculation of relative plant growth and EEF performance to be completed on a daily basis, a more rapid, fully automated approach is required. Machine learning approaches are widely used to process two-dimensional data. However, 3D approaches pose significant additional challenges, and methods to process this data are currently less mature. A specific issue related to 3D data sets is the indeterminate dimensions and point density of point clouds, which require special methods and different models compared to two dimensional data [9].

However, despite the challenges of dealing with 3D point cloud data (PCD's), PCD's have already been used in plant phenotyping via manual and classical artificial intelligence methods [10,11]. Deep learning

* Corresponding author.
E-mail address: matthew.redding@dpi.qld.gov.au (M.R. Redding).

https://doi.org/10.1016/j.atech.2025.101399
Received 28 April 2025; Received in revised form 29 August 2025; Accepted 29 August 2025
Available online 30 August 2025

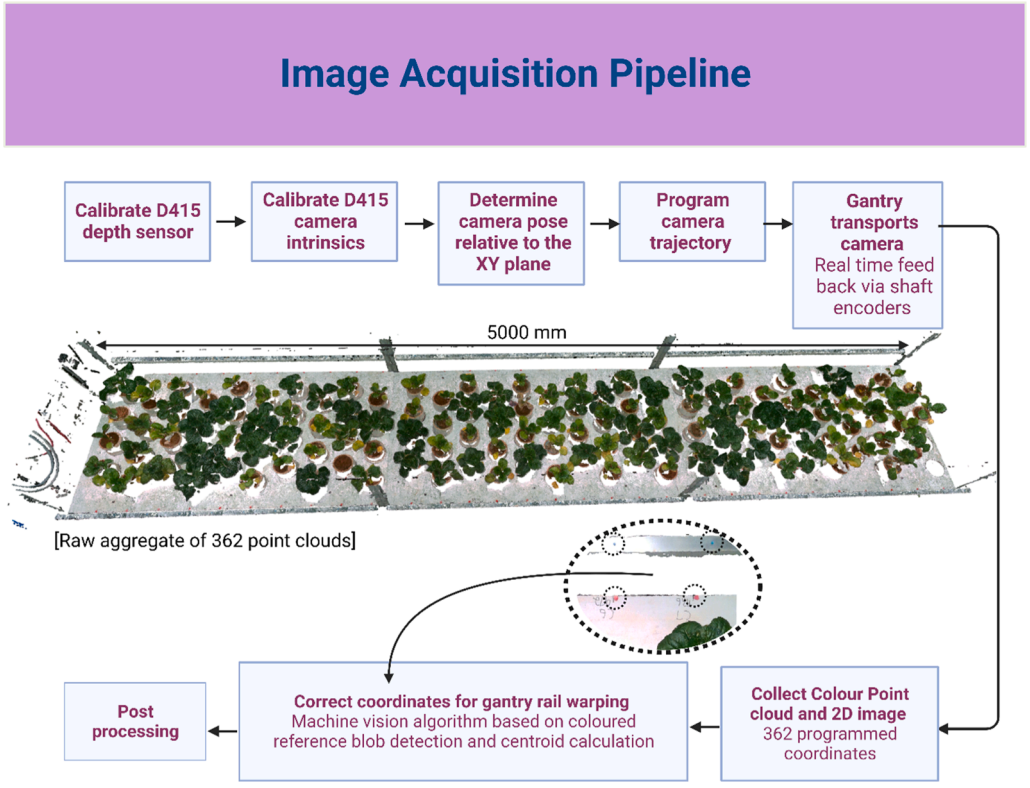

Fig. 1. Data acquisition using the previously described robotic growth accelerator [8]. https://BioRender.com/q42n516.

approaches to plant phenotyping centred around projection or point-based methods have also recently been progressing [10,12]. This includes the recent proof of concept application of the PointNet++ model to deep semantic segmentation of leaves applied to an artificial data-set [13].

Heiwolt et al. [13] were motivated to develop a deep learning approach to phenotyping by the dependence of existing artificial intelligence plant phenotyping methods on hand crafted filters and artificially controlled environments – which lack generalisability or adaptability. Our experience suggests that these same criticism and drawbacks also apply to above ground biomass measurement in the semi-controlled environment of a growth accelerator.

However, rapid scanning to assess above soil biomass in a plant accelerator presents a different requirement to that of phenotyping. Plant structure is not as critical as recognising (segmenting) and counting the above ground biomass. While this is in some ways a less demanding task, ideally it is completed without physically separating the individual plants for scanning. Instead, a camera traverses the densely packed growth accelerator, producing a large volume of data, daily.

Our hypothesis was that we could use an inexpensive 3D camera combined with open-source 3D deep learning libraries and an existing neural architecture to accurately provide automated real-time plant growth measurement. Assessment of the literature surrounding this subject suggests that there are no other existing approaches published, and that the application to the extensive scans we have collected and the labelled training data from real plants is novel.

Materials and methods

Data collection and preprocessing

Data sets were collected during two growth accelerator experiments providing two harvests of bok choy and two of pak choy plants (*Brassica rapa* subsp. *chinensis*) grown on two different soils, and a third experiment using perpetual spinach (*Beta vulgaris* subsp. *cicla* var. *cicla)*. Each of these experiments consisted of replicated Controls (basal nutrients but no nitrogen addition) and a range of treatments (basal nutrients plus various forms of nitrogen additions, each at the same nitrogen rate). Experiment 3 differed from the other two pot experiments, in that a maximum potential dry matter treatment (Potential) was also included. The Potential treatment used the same basal additions, but repeated applications of nitrogen as conventional fertiliser, to remove all nutrient limitations. Water, light, temperature, and basal nutrient additions were supplied at optimum rates.

The robotic growth accelerator used to collect this data has previously been described [8], with the modification that the camera employed is now an Intel Realsense D415 3D camera (Intel Corporation, Santa Clara, CA, USA; https://www.intelrealsense.com/). The process of data acquisition employed following camera depth, pose, and lens calibration involves the camera being transported by the robotic gantry to 362 positions (the camera trajectory) and a point cloud and two-dimensional image being collected from each (Fig. 1). Accuracy of the camera trajectory is ensured through real-time feedback from linear encoders and correction using reference point detection, enabling trajectory coordinates with repeatability of better than 0.2 mm. During plant growth and scanning, temperature was maintained at 25 °C and humidity was controlled via air-conditioning and the continuous operation of a de-humidifier (De Longhi Tasciugo Ariadry) to maintain 50 % relative humidity. Plants were watered 2 h before scanning to ensure full plant turgor. Lighting was mounted to the gantry, adjacent to the camera (0.4 m above the pots), and consisted of six ILS ILH—ON01 white (5700 K) light emitting diodes each driven at 12.25 W (www.i-led.co.uk). During scanning, all grow-lights were de-activated, with the gantry-mounted lights becoming the only source of illumination.

Training and validation of the RandLA-net model

The RandLA-Net model was selected due to its demonstrated performance relative to other point cloud segmentation models [9],

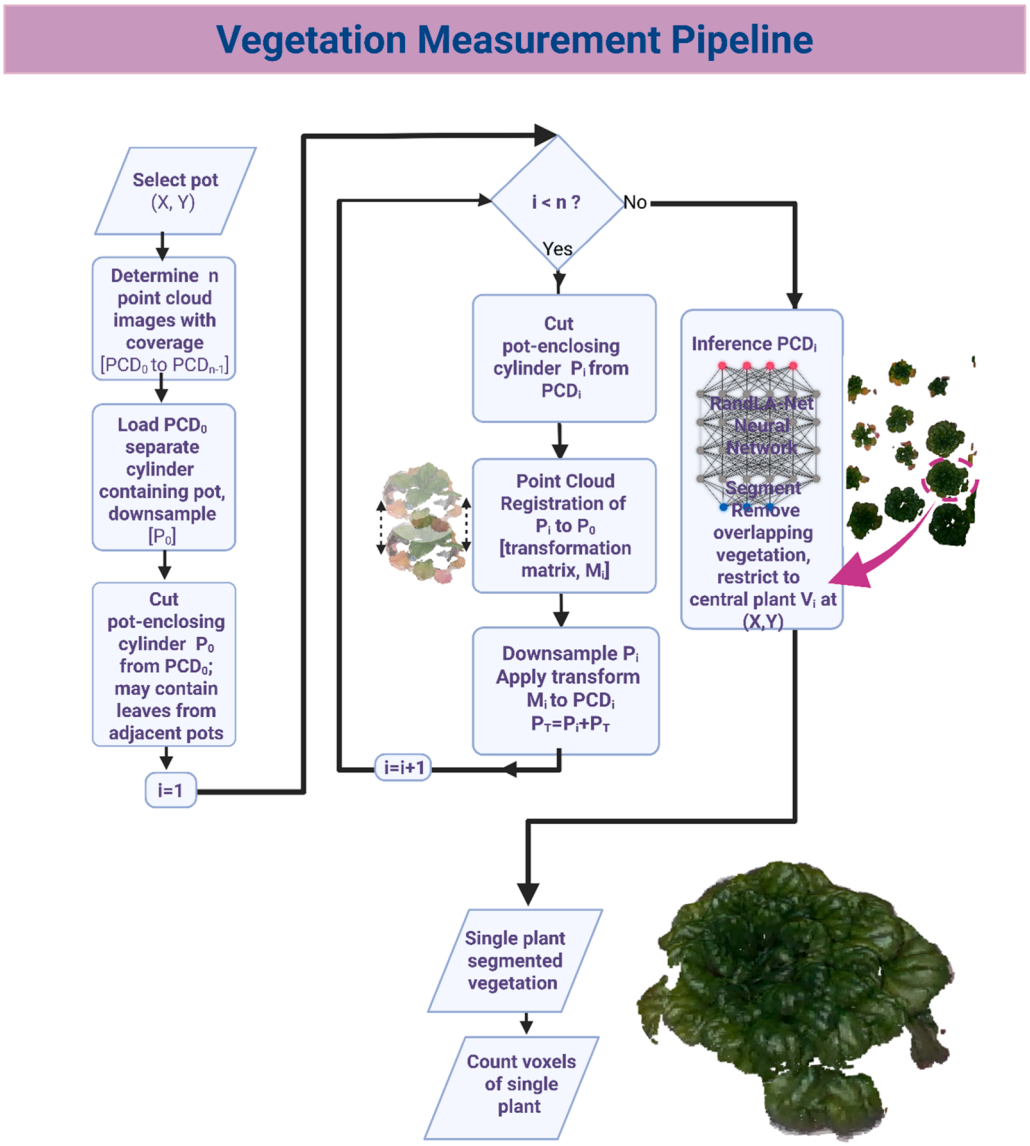

Fig. 2. Summary of the algorithm used to inference the data for an individual pot on a shelf with many other, to calculate its above ground plant matter. https://BioRender.com/q42n516.

particularly its ability to efficiently process large point clouds with limited computational resources. This efficiency is achieved through subsampling large point clouds while preserving feature detail via a local feature aggregation module. While our original point clouds may have around 1 000 000 points, sub-sampling decreased this size to 45, 056 points via the local feature aggregation approach.

Model training focussed on selecting only the vegetation of the central plant (a limited instance segmentation task) from each image containing multiple pots, multiple plants, and growth accelerator infrastructure (e.g. shelving, framework, plumbing, and wiring).

The initial general data set was composed of around 840 PCD files, each image a registered composite of multiple camera poses of a group of pots (each around 3 to 20 MB), and with each point labelled (0: background, including pots, adjacent plants, shelving etc.; 1: central plant vegetation). Images from 7 scanning events were used, collected during the initial two growth accelerator experiments at a range of growth and seedling stages (15/12/2021, 17/12/2021, 20/12/2021, 24/2/2022, 27/7/2022, 15/8/2022, 7/11/2022), in two different soils, with two different plant varieties. A custom program was written using the Open3d [14] and python programming language [15] to facilitate the labelling task.

This data set was randomly divided into training (70 % of images), validation (15 %), and test (15 %) sub-sets. Training was then completed using the framework provided by the machine learning extension to Open3d (Open3D-ML release 0.17; [14]), building a custom data loader for PCD's based on the examples provided. The RandLA-net 3D segmentation deep neural network [9] was randomly initialised, and trained on the data using PyTorch tensor processing [16] in conjunction with Graphics Processing Unit (GPU) exploitation via CUDA (Nvidia [17]). This software was run on an Ubuntu PC (version 20.04.6 LTS) equipped with an Nvidia 3090TI GPU (www.nvidia.com), and i7 central processing unit (www.intel.com) and 128 GB of random access memory.

In addition to the 3D coordinates, we exploit four data features of each point for their inference value: the distance from the centre of the central pot in the image (in the x-y plane), and the colour value of each point (red, green, blue). Up to 200 training epochs were allowed for convergence. Image batch size was adjusted in initial testing to ensure the GPU was operating just below its maximal memory capacity. Inference was conducted on the independent validation set at the end of each training epoch and performance statistics collected (weighted cross-entropy loss [loss], Intersection Over Union for each class [IoU], overall Intersection Over Union, and overall accuracy). Intersection over

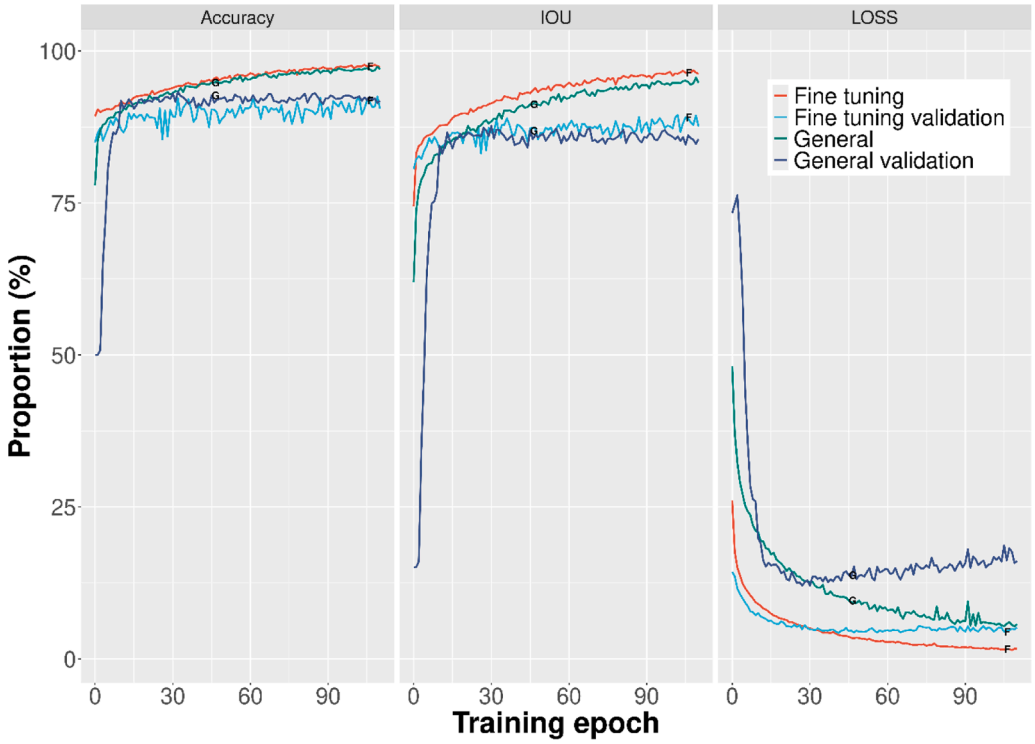

Fig. 3. Training and validation statistics for the training and fine-tuning of the model.

union is calculated as follows:

$$IoU = \frac{Area\ of\ intersection}{Ground\ truth\ area + Predicted\ area - Area\ of\ intersection} \quad (1)$$

A fine-tuning data set was subsequently prepared from 1035 PCD images with a larger weighting to background and pot infrastructure points (collected over about the same period of time as the general composite set) when it became evident that this approach was better suited to the likely deployment requirements for the growth accelerator (Fig. 2). These images were subjected to the identical training process described for the general dataset, however, the learning rate was decreased.

An additional fine tuning was completed using 240 images from scans of the third plant variety ('Perpetual Spinach', *Beta vulgaris* subsp. *cicla* var. *cicla*; images collected from 4 scanning events, 24/4/2024, 14/5/2024, 16/5/2024, and 21/5/2024) to prepare a suitable model to conduct inference on the third pot trial.

The inference and vegetation measurement pipeline

The scanning process involves collection of 362 over-lapping PCD's from a gantry moving across a matrix of x-y coordinates to scan a 1 m X 5 m shelf of up to 120 pots. Accordingly, given a pot-centre x-y coordinate, the vegetation measurement pipeline determines how many images have good coverage of the plant at this pot coordinate (usually about 12 images), registers (aligns) each plant image to the others and returns a composite point cloud, then inferences this composite to extract only the central plant (a partial instance segmentation task). The voxel count of the central plant is then determined. The algorithm implemented is fully represented diagrammatically (Fig. 2). The computation overhead of the point cloud registration task is decreased by limiting registration to z-axis translations (scipy minimise function applied to the sum of distances between points; [18]), a simplification made possible given the high degree of location accuracy of the camera pose determined by the gantry movement and the almost complete overlap of the images. However, approximate global registration followed by more precise iterative closest point registration is also effective though it is more computationally complex

Plant growth comparisons

Plant harvests were compared to prior voxel counts. In addition, since the proposed advantage of this technique is the non-destructive comparison of plant development given different treatments, several comparison approaches were demonstrated.

Firstly, plant voxel profiles over time were compared by fitting the logistic curve, identifying differences in the logistic parameters for different treatments. Secondly, a comparison approach is demonstrated designed to separate treatment effects from some of the limitations of the pot growth approach.

The latter method seeks to use the Control and a maximal production treatment (Potential), in this case with repeated additions of nutrients to achieve optimal growth conditions, as references against which the performance of a treatment is compared at a given day:

$$\text{Proportion of potential} = \frac{(Vox_{Treat} - Vox_{Control})}{(Vox_{Max} - Vox_{Control})} \quad (2)$$

where Vox_{Treat} and $Vox_{Control}$ are the voxel counts for a given day of the treatment and the control respectively; and Vox_{Max} is the maximum overall voxel counts of the Potential comparison.

Statistics

In addition to the evaluation of the validation set each epoch, and the test dataset with the final model, the relationship between plant voxel count and plant above ground dry matter was determined via regression analysis grouped by experiment and harvest using R [19]. Residuals were tested for normality via the Shapiro Wilke test, and a square root transformation applied to the dependent variable where required to achieve normality. The growth profile of the plants (determined from voxel counts) over time was fit via non-linear least-squares regression (nls function) and the self-starting logistic function (SSlogis) using R.

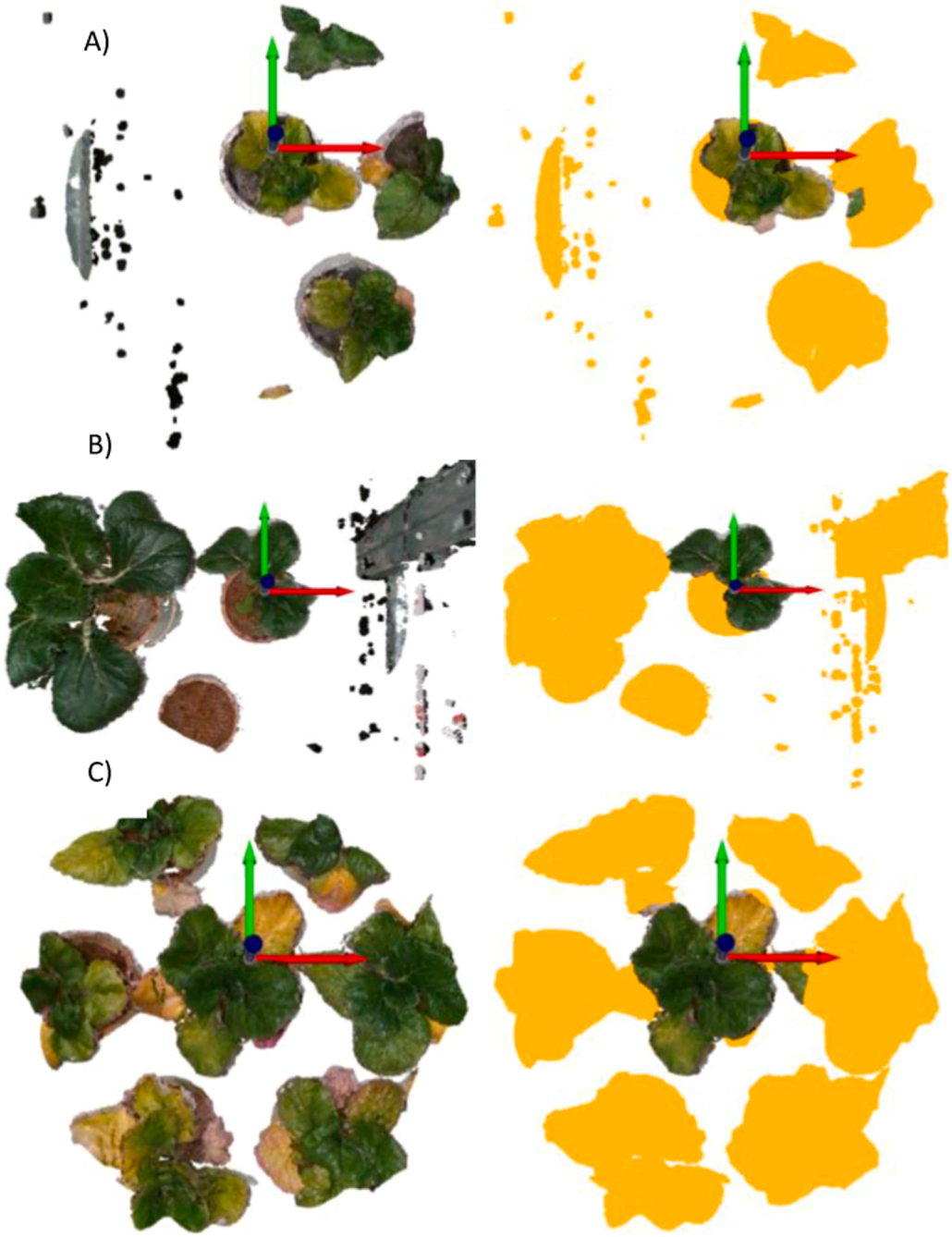

Fig. 4. Three challenging segmentation examples rendered in two dimensions (A,B,C). The cylindrical PCD region on the left is the original, while that on the right has segmented the central plant, while eliminating overlapping plants. Some errors are evident, but the performance is generally adequate (for these three images, accuracy = 0.939, and mean IOU = 0.889). The central plant in each cylindrical PCD is signified by superimposed axes.

Initial parameter estimates were determined using the R function getInitial.

Results

The general data set was used to train the model using a learning rate of 0.00005, with the model parameters from epoch 45 being selected to avoid the over-training indicated by the rise in validation loss (Fig. 3). Fine tuning of this model applied a learning rate of 0.000025, with the 105^{th} epoch parameter values being selected as training loss for the validation set rose after this point. Application of the fine-tuned model to the independent test data set indicated an overall testing accuracy of 0.933 and mean IOU of 0.903, and adequate segmentation of the central plant from other plant material and infrastructure (Fig. 4).

Grouped regression of the square root of above ground dry matter versus plant voxel counts for the four harvests provided a very good linear fit both where different intercepts were allowed for different harvests ($R^2 = 0.865$, $P < 2.2e\text{-}16$; Fig. 5), and where both slopes and intercepts were allowed to independently vary ($R^2 = 0.854$, $P < 2.2e\text{-}16$).

Plant development over time (represented as segmented plant voxels) tended to be well-represented by the logistic curve (Fig. 6), with parameter values, such as the inflection point and upper asymptote, varying with the treatments applied.

Plant scan data from the third experiment was fitted with logistic curves for the Control, Potential, and Treatments 1 and 2 (Fig. 7A). Eq.

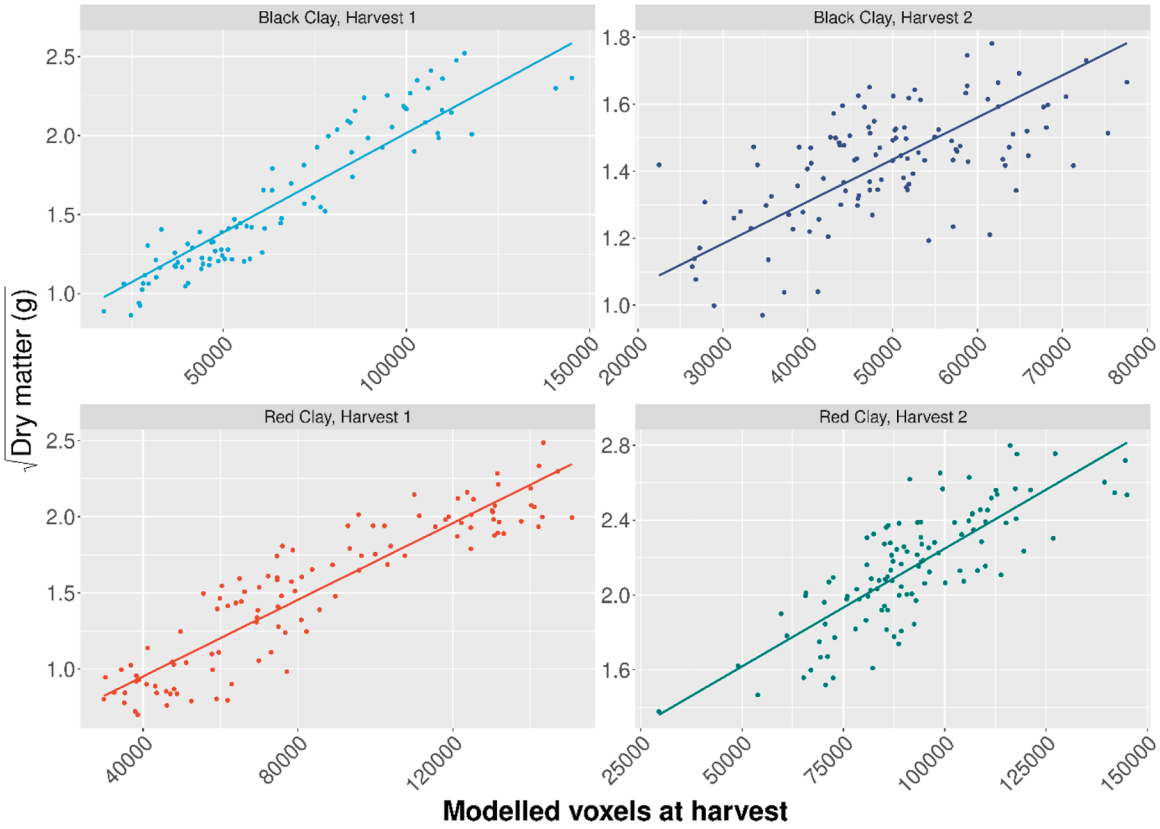

Fig. 5. The relationship between above ground dry matter and segmented voxels determined at harvest.

(1) was applied to this data to enable the time profile of nutrient delivery relative to the two references (Control and Potential) to be displayed (Fig. 7B).

The automated processing of 362 PCD's from a single scan (segmenting 120 pots), consumed about 102 min, with each individual PCD inference using the RandLA-net model consuming about 0.7 s. Profiling the code for the registration, inference (Fig. 2), and treatment voxel counting portion of the pipeline suggests that the inferencing step consumes about 26 % of the execution time. Labelling 100 PCD's to create a fine-tuning data set requires about 10 h of staff labour.

Discussion

The observed training statistics were acceptable (Fig. 3). The inclusion of the data features (red, green, blue, and distance from the centre) enabled sufficiently accurate segmentation of the central plant instance (Fig. 4) to successfully validate the relationship versus harvest data (Fig. 5). The model and pipeline performed adequately to characterise growth over time and discern differences between treatments, with a demonstrated ability to fit logistic growth curves to the measured plant data (Fig. 6). The technique also enables key statistics related to the time profile of nutrient delivery of plants to be measured (e.g. the days to the inflection point of the logistic curve).

Therefore, the technique is suitable for the investigation of nutrient delivery synchronisation with the plant nutrient demand. The study described here applied the techniques to nitrogen delivery from various fertiliser forms. However, it could be applied to another nutrient of interest.

To optimise the technique for synchronisation investigations, a clear understanding of the demand profile of the target plant is required. The most appropriate model plant in nutrient uptake synchronisation studies, as described here, may not be the target plant for the economic application of the fertiliser. The model plant should exhibit a maturation period that exceeds the key synchronization period of the target plant – or at least long enough to show an improvement relative to conventional fertilisers.

The inclusion of maximum potential treatments in experiment 3 enabled better evaluation of synchronisation and the effective nutrient supply profile of a treatment (Fig. 7). Other treatments should then aim to limit supply so that plant growth does not reach this potential, is non-asymptotic throughout the experiment, and unlimited by phenotype and the experimental system. For example, nutrient applications rates could be selected to achieve two-thirds of the uptake:

$$N_{Treat} \approx \frac{2}{3}\left(Asym_{Potential} - Asym_{Control}\right), \quad (3)$$

where, N_{Treat} is the nutrient application rate, $Asym_{Potential}$ and $Asym_{Control}$ are the nutrient uptake at the asymptote for the Potential treatment and the Control respectively.

This deep learning approach to processing the PCD's allows a considerable improvement to data analysis throughput. Previously the use of K-nearest neighbour clustering techniques required around 2 h to process each full shelf scan (120 pots; as completed previously for [8]), with full attention from a staff member to conduct this work. Allowing 10 h to prepare a fine-tuning data set for an experiment, the deep learning approach only requires 18 % as much staff time per experiment (28 scans). With the modestly specified computer applied in this case, inferencing each scan of 362 images was complete within about 36 min.

In many ways the research question this technique can answer is a simpler one than is answered by artificial intelligence phenotyping techniques (e.g. [10]). Given the environmental threats posed by the poor efficiency of conventional fertilisers [20], and the economic impact of wasted nutrients, a technique to improve research throughput in nutrient supply synchronisation studies is of significant value.

The current data acquisition and inference pipeline measures a surrogate of dry matter production. Our current research focus is to extend

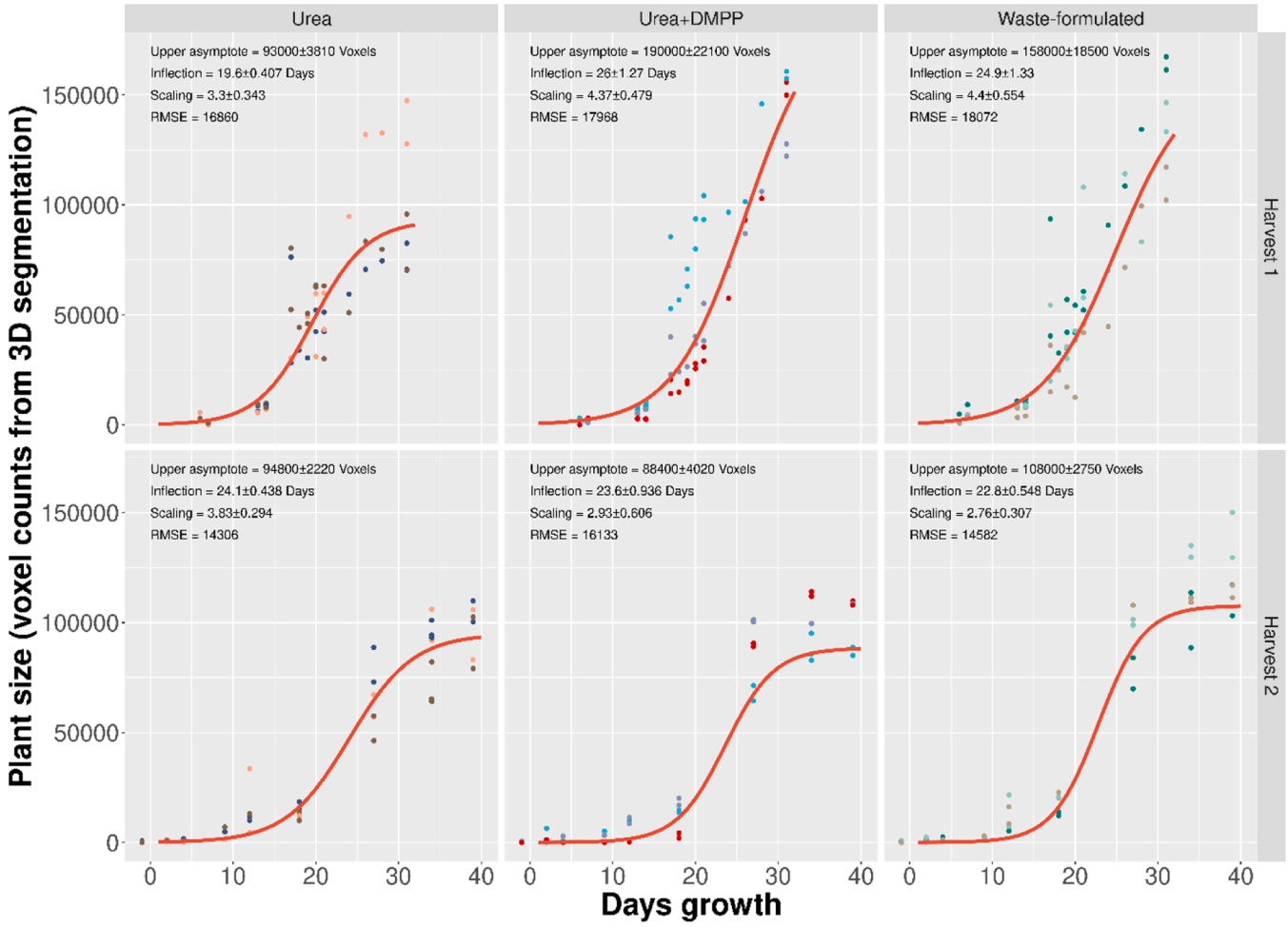

Fig. 6. Example growth profiles of above ground plant size versus days growth (experiment 2). Statistics of the presented logistic fits are included on each facet (mean ± standard error, $P < 0.001$ for all parameter estimates; Root Mean Square Error, RMSE, is marked on each panel), demonstrating the capacity to differentiate statistically between the time profiles of treatments.

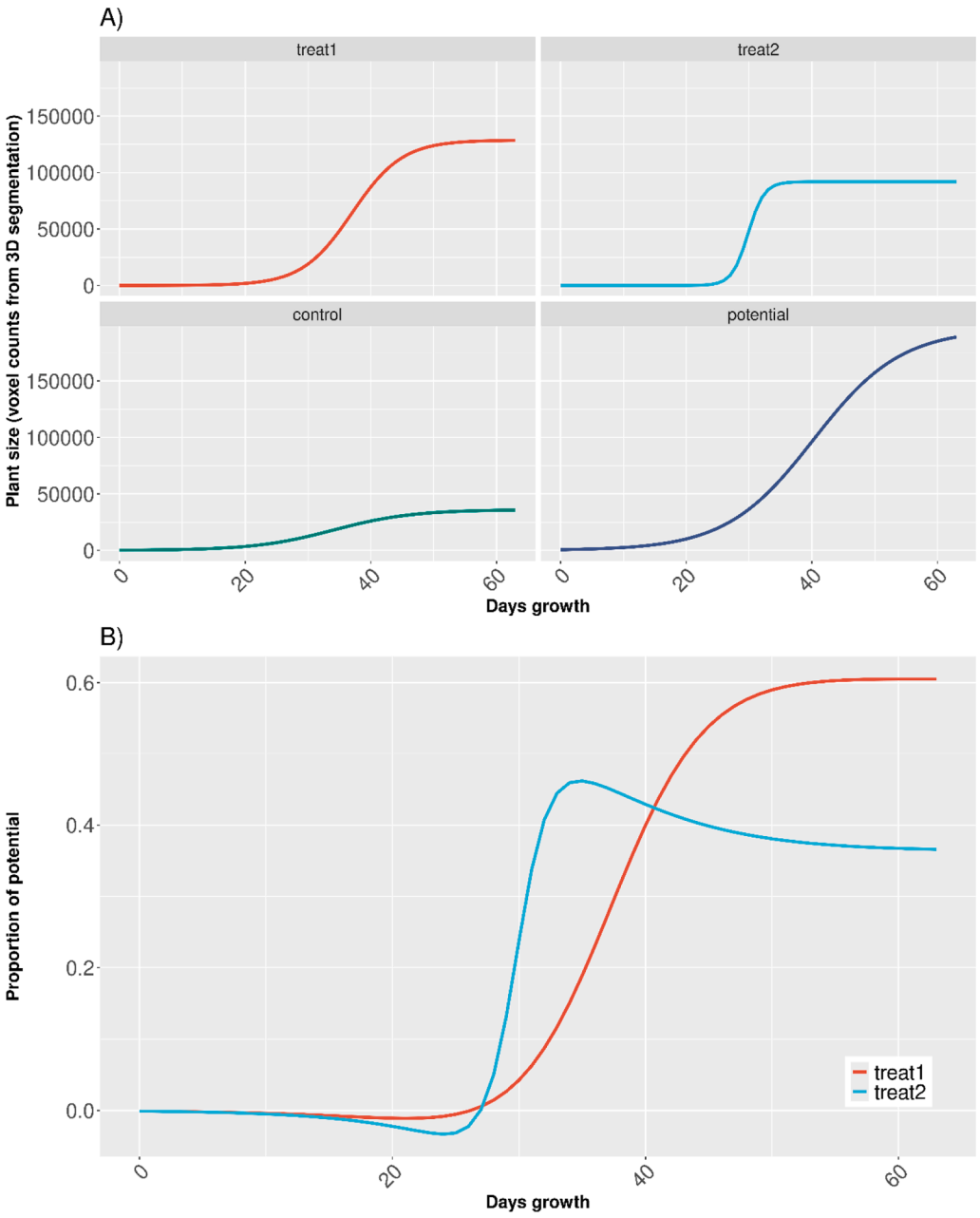

Fig. 7. An application of Eq. (2) to enable the simplification of the comparison of two treatments to the references (Control and Potential; panel A) to just two curves (panel B; based on treatments from experiment 3).

the sensing capabilities to enable measurements of above ground biomass nitrogen content.

CRediT authorship contribution statement

Matthew R. Redding: Writing – review & editing, Writing – original draft, Visualization, Validation, Supervision, Software, Resources, Project administration. **Armando J. Navas Borrero:** Writing – review & editing, Software, Data curation.

Declaration of competing interest

No conflicts of interests or competing interests affect this study to the best knowledge of the authors.

Acknowledgements

I would like to thank Dr Sheikh Rabbi for his advice during manuscript preparation.

Data availability

The checkpoint (parameter weights) for the trained model, example data loader, and example images are available on request.

Ethics Statement

Not applicable: This manuscript does not include human or animal research.

Data availability

The checkpoint (parameter weights) for the trained model, example data loader, and example images are available on request.

References

[1] X. Chen, F. Zhang, V. Römheld, D. Horlacher, R. Schulz, M. Böning-Zilkens, P. Wang, W. Claupein, Synchronizing N supply from soil and fertilizer and N demand of winter wheat by an improved Nmin method, Nutr Cycl Agroecosyst 74 (2006) 91–98, https://doi.org/10.1007/s10705-005-1701-9.

[2] X.P. Chen, F.S. Zhang, Z.L. Cui, F. Li, J.L. Li, Optimizing soil nitrogen supply in the root zone to improve maize management, Soil Sci. Soc. Am. J 74 (2010) 1367–1373.

[3] M.R. Redding, R. Lewis, T. Kearton, O. Smith, Manure and sorbent fertilisers increase on-going nutrient availability relative to conventional fertilisers, Sci. Total Environ. (2016) 927–936, https://doi.org/10.1016/j.scitotenv.2016.05.068, 569–570.

[4] G. Gillman, A. Noble, Environmentally manageable fertilizers: a new approach, Environ. Qual. Manag. 15 (2005) 59–70.

[5] M.R. Redding, I. Phillips, C. Pratt, C. Paungfoo-Lonhienne, I. Levett, J. Hill, C. Mehta, T. Bailey, R. Brackin, J. McAuley, S. Pratt, B. Laycock, D.G. Mayer, Can nitrogen source and nitrification inhibitors affect In-season nitrogen supply? Commun. Soil Sci. Plant Anal. 51 (2020) 2189–2204, https://doi.org/10.1080/00103624.2020.1822383.

[6] J. Lu, Y. Li, Y. Cai, P. Jiang, B. Yu, Co-incorporation of hydrotalcite and starch into biochar-based fertilizers for the synthesis of slow-release fertilizers with improved water retention, Biochar 5 (2023) 44, https://doi.org/10.1007/s42773-023-00242-w.

[7] A. Rashidzadeh, A. Olad, A. Reyhanitabar, Hydrogel/clinoptilolite nanocomposite-coated fertilizer: swelling, water-retention and slow-release fertilizer properties, Polym. Bull. 72 (2015) 2667–2684, https://doi.org/10.1007/s00289-015-1428-y.

[8] M.R. Redding, T. Witt, C.R. Lobsey, D.G. Mayer, B. Hunter, S. Pratt, N. Robinson, S. Schmidt, B. Laycock, I. Phillips, Screening two biodegradable polymers in enhanced efficiency fertiliser formulations reveals the need to prioritise performance goals, J. Env. Manage 304 (2022) 114264, https://doi.org/10.1016/j.jenvman.2021.114264.

[9] Q. Hu, B. Yang, L. Xie, S. Rosa, Y. Guo, Z. Wang, N. Trigoni, A. Markham, RandL a-net: efficient semantic segmentation of large-scale point clouds, arXiv e-prints (2019), https://doi.org/10.48550/arXiv.1911.11236. arXiv:1911.11236.

[10] N. Harandi, B. Vandenberghe, J. Vankerschaver, S. Depuydt, A. Van Messem, How to make sense of 3D representations for plant phenotyping: a compendium of processing and analysis techniques, Plant Methods 19 (2023) 60, https://doi.org/10.1186/s13007-023-01031-z.

[11] S. Paulus, H. Schumann, H. Kuhlmann, J. Leon, High-precision laser scanning system for capturing 3D plant architecture and analysing growth of cereal plants, Biosyst. Eng. 121 (2014) 1–11, https://doi.org/10.1016/j.biosystemseng.2014.01.010.

[12] S. Jin, Y. Su, S. Gao, F. Wu, T. Hu, J. Liu, W. Li, D. Wang, S. Chen, Y. Jiang, S. Pang, Q. Guo, Deep learning: individual maize segmentation from terrestrial lidar data using faster R-CNN and regional growth algorithms, Front. Plant Sci. 9 (2018), https://doi.org/10.3389/fpls.2018.00866.

[13] K. Heiwolt, T. Duckett, G. Cielniak, Deep semantic segmentation of 3D plant point clouds, in: C. Fox, J. Gao, A. Ghalamzan Esfahani, M. Saaj, M. Hanheide, S. Parsons (Eds.), Towards autonomous robotic systems, Springer International Publishing, Cham, 2021, pp. 36–45.

[14] Q.Y. Zhou, J. Park, V. Koltun, Open3D: a modern library for 3D data processing, arXiv:1801.09847 (2018).

[15] G. Van Rossum, F.L. Drake. Python 3 reference manual. CreateSpace, Scotts, Valley, CA, 2009.

[16] Paszke, A., Gross, S., Massa, F., Lerer, A., Bradbury, J., Chanan, G., Killeen, T., Lin, Z., Gimelshein, N., Antiga, L., Desmaison, A., Köpf, A., Yang, E., DeVito, Z., Raison, M., Tejani, A., Chilamkurthy, S., Steiner, B., Fang, L., Bai, J., Chintala, S., 2019. PyTorch: an imperative style, high-performance deep learning library. arXiv:1912.01703. https://doi.org/10.48550/arXiv.1912.01703.

[17] Nvidia Developer, 2022. CUDA Toolkit V11.8 Document]. https://developer.nvidia.com/cuda-11-8-0-download-archive. developer.nvidia.com/cuda-11-8-0-download-archive (accessed 12.20.23).

[18] P. Virtanen, R. Gommers, T.E. Oliphant, M. Haberland, T. Reddy, D. Cournapeau, E. Burovski, P. Peterson, W. Weckesser, J. Bright, S.J. van der Walt, M. Brett, J. Wilson, K.J. Millman, N. Mayorov, A.R.J. Nelson, E. Jones, R. Kern, E. Larson, C. J. Carey, İ. Polat, Y. Feng, E.W. Moore, J. VanderPlas, D. Laxalde, J. Perktold, R. Cimrman, I. Henriksen, E.A. Quintero, C.R. Harris, A.M. Archibald, A.H. Ribeiro, F. Pedregosa, P. van Mulbregt, SciPy 1.0: fundamental algorithms for scientific computing in Python, Nat. Methods 17 (2020) 261–272, https://doi.org/10.1038/s41592-019-0686-2.

[19] R Core Team, R: A language and environment for statistical computing, R Foundation for Statistical Computing, Vienna, Austria, 2020.

[20] L.E. Drinkwater, S.S. Snapp, Nutrients in agroecosystems: rethinking the management paradigm, Adv. Agron. Vol. 92 (2007) 163–186.